ACS APPLIED MATERIALS & INTERFACES

Research Article

www.acsami.org

Nanoparticle Adhesion and Mobility in Thin Layers: Nanodiamonds As a Model

Magdalèna Couty, Hugues A. Girard,* and Samuel Saada

CEA, LIST, Diamond Sensors Laboratory, F-91191 Gif-sur-Yvette, France

Supporting Information

ABSTRACT: Small size and enhanced properties of nanoparticles (NP) are great advantages toward device miniaturization. However, adhesion is essential for the reliability of such NP layer-based devices. In this work, we present some quick tests to investigate the adhesion behavior of the whole NP layer by mimicking several applicative environments: biological buffers and cells, corrosion, and microfabrication processes. This statistic approach evaluates both adhesion and mobility respectively through particle density and layer homogeneity. We chose nanodiamonds (ND) as reference particles because they are spherical and inert and exhibit either positive or negative zeta potential for the same diameter while surfactant-free. Several deposition methods were used to prepare a wide range of ND layers with various densities and size distribution. We found some unexpected results confirming that the deposition method has to be carefully selected according to the targeted application. A selection of the suitable method(s) to prepare ND layers which are resilient in their applicative environment can be done based on these results. However, ND adhesion still remains critical in some conditions and thus requires further improvement. Most important, this study points out that NP adhesion behavior is more complex than simple particle detachment—or not—from the surface. The particles could also reorganize themselves in clusters. We evidenced, in particular, a surprising mobility driven by air/water interfaces during evaporation of water microdroplets. Further comparison with other materials would indicate if the highlighted phenomena could be extended to any nanoparticles layer.

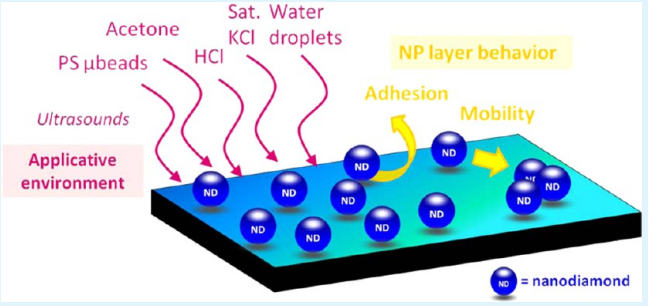

KEYWORDS: *nanoparticles, nanodiamonds, thin layer, adhesion, mobility*

1. INTRODUCTION

Thanks to the research efforts led these last years on the comprehensive technology of nanoparticles (NP), it is now possible to prepare highly dense and homogeneous thin layers on various large scale substrates.[1] NP layers offer an alternative to thin films of the same material on delicate substrates unable to undergo deposition processes at high temperature or in reactive environments such as plasmas. Moreover, they often exhibit enhanced properties thanks to specific phenomena related to the nanoscale (i.e., high surface-to-volume ratio). Some well-known examples are the better performance of gold NP for surface plasmon resonance[2] and the use of transition-metal NP for heterogeneous catalysis.[3] Small size and enhanced properties of NP are great advantages toward device miniaturization and batch fabrication. However, the reliability of such devices strongly depends on the layer adhesion.

Adhesion of nanosized particles on a substrate and their interactions with this latter have been the object of many theoretical studies and mechanisms investigations by simulation.[4−7] Experimentally, the main method for adhesion study is atomic force microscopy (AFM), allowing quantitative force measurements directly on single particles in air, nitrogen and even in liquids.[8−10] Conventional adhesion tests including pull-off, lateral push,[11] bending and scratch[12] tests provide information on a larger number of particles but require sample preparation and are often limited by the setup itself—for instance, the adhesive strength of glue in the case of tensile test. Laser shock adhesion test has been recently developed[13] but is complex to implement and not suitable for all substrates.[14] In this paper, we aim to present a set of quick adhesion tests, easy to perform, to investigate the adhesion behavior of NP layers in some applicative environments.

We chose diamond NP or "nanodiamonds" (ND) as a model of nanoparticles in this study. These particles are composed of an inert sp3 carbon core[15] covered only with chemical moieties conferring them a positive or negative zeta potential.[16] Thanks to this intrinsic zeta potential, they can be dispersed in water[17] without the use of any surfactant or other stabilizing agents which may add an undesired contribution to adhesion layer behavior. In particular, we used colloidal suspensions of spherical ND of the same diameter, produced by detonation process,[18] one exhibiting a negative zeta potential and the other a positive one.

Received: March 17, 2015
Accepted: July 7, 2015
Published: July 7, 2015

DOI: 10.1021/acsami.5b02364
ACS Appl. Mater. Interfaces 2015, 7, 15752−15764

Scheme 1. Deposition Methods Used to Prepare ND Layers

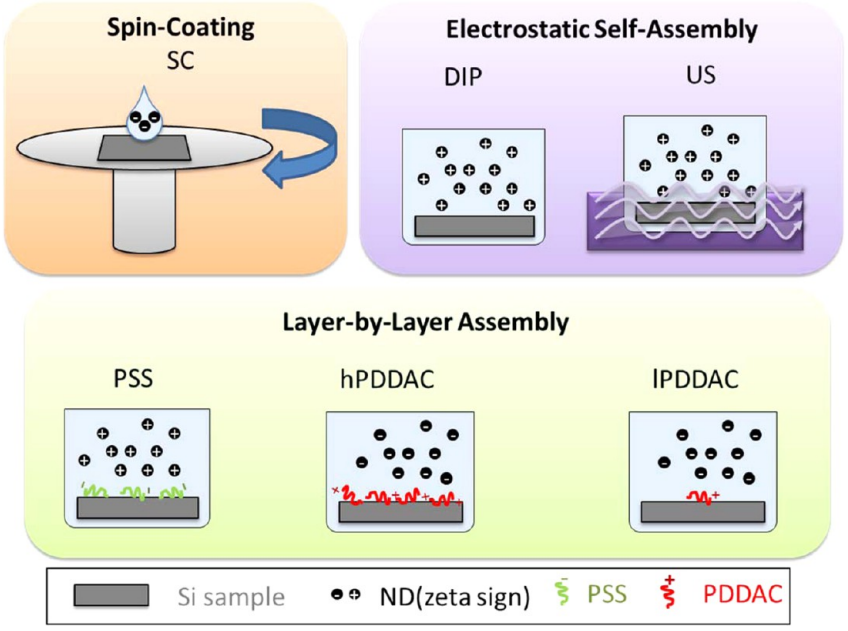

ND have become one of the most promising nanocarbon these last years due to their exceptional physical, chemical, biological, mechanical and optical properties. Their structure ensures a high chemical resistance while offering a versatile surface chemistry.[19] Stable fluorescence properties could be also introduced through nitrogen vacancy centers created by irradiation and annealing.[20−22] A large number of in vitro and in vivo studies have confirmed that ND have very low cytotoxicity on numerous cell lines including osteoblasts and neuroblasts, glial and marrow, liver, kidney, intestine and lung cells.[23−27] Further than simple biocompatibility due to chemical inertness, Thalhammer et al. reported that an ND monolayer coating even promotes the formation of a functional neuronal network.[28,29] Finally, diamond nanoparticles exhibit excellent tribological properties.[18,30−32] All the properties mentioned above make ND highly desirable for a wide range of applications in various fields, either dispersed in colloids or deposited on a surface. The latter case includes seeding prior to film growth by chemical vapor deposition (CVD),[33−38] protective coatings against corrosion,[39,40] tissue scaffold engineering,[41,42] platforms for protein immobilization on biosensors,[43] sensitive coatings for surface acoustic wave sensors[44] and attachment to probe for nitrogen-vacancy center mapping.[45]

Numerous methods have been reported for ND deposition: drop casting,[46] electrophoresis,[40,47,48] spin-coating (SC),[36,37,49] electrospray deposition,[50] electrostatic self-assembly,[36,51−55] covalent grafting,[56−58] microcontact printing,[59,60] inkjet printing,[61,62] and so on. Each one offers its own advantages and drawbacks thus there is no single best approach to deposit ND on a substrate. The most suitable method should be chosen according to the substrate properties, including the material itself, size, and geometry, and to the targeted layer characteristics in terms of density and size distribution (isolated particles, clusters, or both), homogeneity, adhesion, and surface chemical availability. For instance, electrophoresis is limited to conducting substrates and its implementation requires specific optimization almost for each sample size and geometry while SC allows for ND deposition on large scale substrates without material limitation maybe except for its wettability, but is not compatible with 3D structures. The use of intermediate polyelectrolyte layers has been reported in particular for 3D nanostructures covering with a dense and highly homogeneous ND layer.[51]

As for any other NP, ND layer adhesion could be critical for the subsequent application and the device durability. For instance, if the ND layer is prepared for molecule immobilization on a sensor, it has to be adherent enough in the functionalization medium that could be an organic solvent, in the presence of base or acid. Even in the case of bioconjugation for protein grafting, the coupling medium is often a buffer containing different kinds of ions. Another example is the aging of the layer, that is, the number of cycles a device can endure before performance decrease and the effects of storage time and environment between two uses. However, ND adhesion remains poorly studied. To our best knowledge, only two teams have reported such studies. Lu et al. grafted fluorinated ND onto silanized glass and measured ND friction and adhesion properties using AFM both in ambient and dry nitrogen environment.[63] Very recently, adhesion forces between sharp silicon AFM tips and ND were investigated by Aravind et al.[64] The authors found dependence on purity of particles, size of the probe, and environmental conditions.[65]

We propose here a statistic approach evaluating the adhesion of the whole layer exposed to soft or harsh conditions by mimicking environments of some biological and technological applications: saturated KCl as a simple model of buffers with a high ionic strength, acetone as polar organic solvent commonly used in clean-room processes such as lift-off and cleaning, PS beads similar to cells in terms of size and Young's modulus, HCl 0.1 M as a corrosive medium for protective coatings, condensation and evaporation of water microdroplets traducing sample aging. We aim at screening a large range of layers prepared with ND of the same diameter (core 5 nm) exhibiting either positive or negative zeta potential and deposited on silicon using different methods: spin-coating or electrostatic self-assembly with or without a polyelectrolyte intermediate layer or assisted by ultrasounds. Both a semiquantitative

DOI: 10.1021/acsami.5b02364
ACS Appl. Mater. Interfaces 2015, 7, 15752−15764

Scheme 2. Principle of the Microdroplet Test

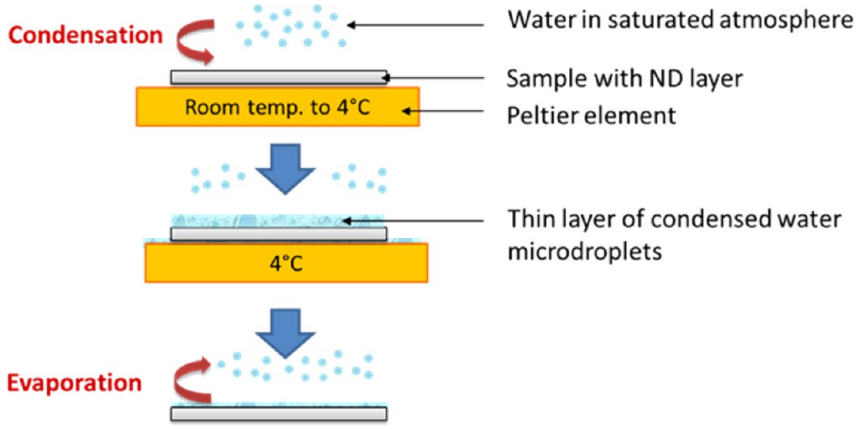

evaluation of NP adhesion through the particle density evolution and a qualitative evaluation of their mobility through the layer homogeneity are given. These results can help to select suitable deposition methods ensuring the required adhesion for the targeted ND layer application.

2. EXPERIMENTAL SECTION

2.1. Materials. Two aqueous colloids of detonation ND were used. The first one, referred as "ND(−)", is a commercial slurry "ND-H2O-5N" from Adámas Nanotechnologies, Inc. (Raleigh, NC,). The other, referred as "ND(+)", was provided by the NanoCarbon Research Institute Co., Ltd. (Japan). Both solutions were only submitted to simple processes such as dilution and sonication for 1 h at 240 W with Hielscher UP400S, 24 kHz. The final working concentration was 0.1 wt % Ultrapure water with a resistivity of 18.2 MΩ.cm at 25 °C was obtained from a Milli-Q apparatus (Millipore) and used for all experiments. Polydimethyldiallylammonium chloride or PDDAC (Mw = 100 000−200 000 g/mol) 20 wt %in water, poly(sodium-4-styrenesulfonate) or PSS (Mw = 1 000 000 g/mol), polystyrene (PS) beads 2 μm in diameter were purchased from Sigma-Aldrich. Potassium chloride, hydrochloric acid 37% were provided by VWR. Acetone was supplied by Carlo Erba.

2.2. ND Characterization. Hydrodynamic diameters and zeta potentials of the particles were measured at pH 7 and 25 °C by Dynamic Light Scattering (DLS) with a Malvern Zetasizer Nano ZS instrument at 173° angle.

High-Resolution Transmission Electron Microscopy (HRTEM) observation of ND(+) was carried out using an FEI Tecnai F20 field emission gun microscope operating at 200 kV and equipped with a Gatan Imaging Filter. A drop of NDs dispersed in methanol was deposited on a 3 mm diameter copper grid covered with a holey carbon film. Images were taken near the Scherzer focalization (−63 nm) using a (1k × 1k) CCD camera. Local area fast Fourier transform diffractograms, equivalent to electron diffraction patterns, were exploited in order to determine structural and crystallographic characteristics of the observed NDs. HRTEM image of ND(−) is a courtesy of Bogdan Palosz, Institute of High-Pressure Physics, Warsaw, Poland.

A Nicolet 8700 FT-IR Spectrometer from ThermoScientific, equipped with a DGTS detector, set at resolution 4 cm^{-1} was used for FTIR measurements. A drop of ND suspension was dried in a crucible then milled with KBr to prepare the pellet. Direct single-path transmission measurements were performed after drying overnight at 50 °C in a thermostat chamber under vacuum to avoid water and CO_2 interferences during the spectra collection.

2.3. Preparation of ND Layers. ND were deposited on (100) silicon samples about 1 cm^2 in size, previously cleaned 5 min in PIRANHA solution. Several methods including spin-coating, electrostatic self-assembly and layer-by-layer have been screened (Scheme 1). Layers referred as "SC" were prepared by spin coating ND(−) at a spin rate of 3000 rpm for 20 s. Drying was completed in an oven at 60 °C for 30 min. Four electrostatic self-assembly variants were investigated. Layers referred as "DIP" were prepared by sample immersion in ND(+) for 30 min then gently rinsed with water and dried under nitrogen flow. The same process carried out in an ultrasonic bath was used to prepare the samples with electrostatic self-assembly assisted by sonication, referred as "US". Two kinds of ND layers were deposited using a polyelectrolyte intermediate layer. The first one was prepared by immersion for 20 min in PDDAC solution, rinsing with water then directly plunged into ND(−) for 20 min and finally rinsing and drying under nitrogen flow. Two polyelectrolyte concentrations (2 μg/mL and, 2 mg/mL respectively referred as "lPDDAC" and "hPDDAC") were used to vary particle density and size distribution. The same process with PSS at 2 mg/mL and ND(+) was carried out for the preparation of "PSS" samples.

2.4. Adhesion Testing. Two kinds of adhesion tests were performed: sonication and condensation/evaporation of water microdroplets. In the first case, samples underwent 1 h of sonication in one of the following media: saturated KCl, acetone, PS beads Ø 2 μm at 0.1 wt % in water, HCl 0.1 M. The maximal temperature recorded was 56 °C. NaOH 0.1 M as the basic condition was not included in the test set because resulting in silicon etching. In the second case, a setup was developed to induce condensation and evaporation of water microdroplets in controlled conditions. It consists in cooling the sample with ND layer from room temperature to 4 °C by thermoelectric effect using a Peltier element (Scheme 2). The Peltier element was placed in a glove compartment with a humidifier to ensure atmosphere saturation. Condensation of water microdroplets from this ambient humidity spontaneously occurred on the sample when its temperature was below 7 °C. Then, the sample was removed from the Peltier element and the micro droplets evaporated while the sample was quickly retrieved room temperature. The thermal conductivity of silicon allowed droplet evaporation in 10 s.

2.5. SEM Observation. ND layers were observed by SEM with a Carl Zeiss AG Supra-40 microscope. Pictures were recorded using an in-lens detector at acceleration voltages of the incident primary electron beam of 6 or 20 kV and a working distance of 4 mm. Images presented in this article have not sustained any modification except for simple contrast and brightness adjustments. Densities were determined by image analysis with ImageJ software. A binary picture (black/white) was obtained from the gray-level image by applying a threshold. This latter has only a slight impact on density value: it varies about 5% when the threshold is 6 gray-levels higher or lower. The objects on the binary image were then counted by scanning the image until it finds the edge of an object. We chose a counting method based on the relative area of objects to avoid misestimating due to aggregation. The density was calculated by dividing the number of particles by the defined area. For each sample, images of three different areas were analyzed. Only the average value and standard deviation were considered further in the study.

DOI: 10.1021/acsami.5b02364
ACS Appl. Mater. Interfaces 2015, 7, 15752−15764

3. RESULTS AND DISCUSSION

3.1. Nanodiamonds Characterization. Nanodiamonds are chosen here as a model nanoparticle to study the adhesion behavior of NP layers according to the deposition method and the environment. In particular, two aqueous colloids of detonation ND with a very close hydrodynamic diameter (Table 1; see Supporting Information, Figure S1 for DLS measurements) were used in the study. They exhibit intrinsic zeta potential of opposite signs (Table 1; see Supporting Information, Figure S2 for DLS measurements) thus are respectively called ND(−) and ND(+).

Table 1. Mean Size and Zeta Potential of the ND

solution	mean size (nm)	zeta potential (mV)
ND(−)	5	−52
ND(+)	8	+35

HRTEM images in Figure 1 show the crystalline structure of the spherical sp^3 carbon core for both ND types. The particle sizes on these images are consistent with the DLS measurements. ND(+) "as received" (image reprinted with permission from ref 66) present a diamond core of approximately 5 nm, with an interplane distance of 2.06 Å which is characteristic of (111) diamond planes. This core is covered by a disordered amorphous carbon shell thinner than 1 nm. Note that no organized graphitic structures could be clearly distinguished on the surface. ND(−) present a diamond core similar in size with almost no visible shell, probably thanks to further purification processes.

As the intrinsic zeta potential of ND originates mainly from their surface groups, their dispersion in water is possible without the use of surfactant. We investigated the surface chemistry of both ND types by FTIR characterization (Figure 2). Corresponding peak assignments are given in Table 2. Most peaks are common to both spectra. The three bands between 1100 and 1300 cm^{-1} correspond to intrinsic diamond bands[18] though the first one could also be attributed to C−O−C bonds in ether, anhydride, lactone or epoxy groups. The bands from 2850 to 2960 cm^{-1} are related to symmetric and asymmetric stretching of CH_2 and CH_3 in alkyl chains, probably from alkanes adsorbed at the ND surface. Two bands appear at 1640 and 3300−3400 cm^{-1}, respectively O−H bending and stretching in hydroxyls groups and eventually in residual adsorbed water in spite of drying overnight under vacuum at 50 °C (Supporting Information, Figure S4). The main difference between the spectra is the position of the carbonyl peak due to C═O stretching, at 1720 cm^{-1} for ND(+) while at 1780 cm^{-1} for ND(−). Tu et al. demonstrates that C═O stretching frequency on ND surface is dependent on the particle size,[67] but in our case both ND types have similar diameters so the comparison is relevant. Shenderova et al. attributed the carbonyl peak at 1725 cm^{-1} to unsaturated anhydrides[68] (already present before drying; Supporting Information, Figure S4) and the one at 1787 cm^{-1} to lactones.[69]

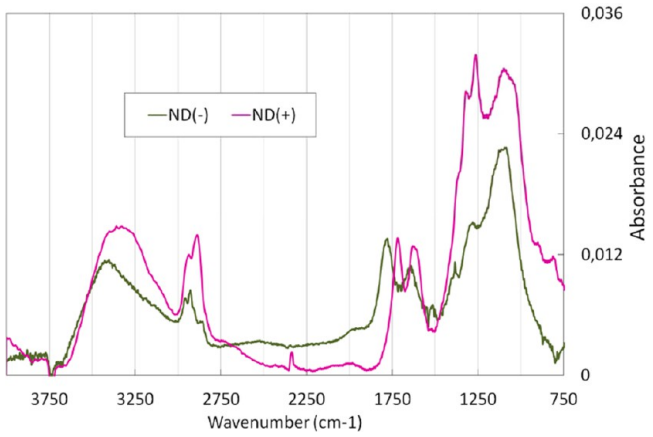

Figure 2. FTIR spectra of ND(−) and ND(+).

Table 2. Peak Assignments for FTIR Analysis

wavenumber (cm^{-1})		
ND(−)	ND(+)	peak assignment
1096	1120	C−O−C bonds in ether, anhydride, lactone and/or epoxy groups
1096, 1280	1120, 1263, 1321	diamond intrinsic bands
1641	1622	O−H bending in hydroxyls groups and residual adsorbed water
1780	1720	C═O stretching in carbonyls
2850, 2925, 2960	2885, 2940	CH_3 and CH_2 symmetric and asymmetric stretching in alkyl chains
3423	3334	O−H stretching (H-bonded) in hydroxyls and residual adsorbed water

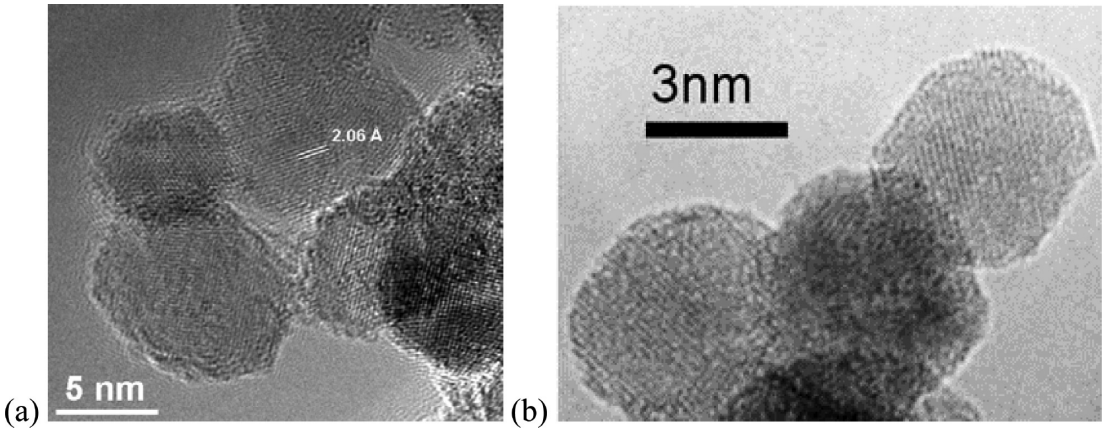

Figure 1. HRTEM images of (a) ND(+), reprinted with permission from ref 66, and (b) ND(−), courtesy of Bogdan Palosz, Institute of High Pressure Physics, Warsaw, Poland.

DOI: 10.1021/acsami.5b02364
ACS Appl. Mater. Interfaces 2015, 7, 15752−15764

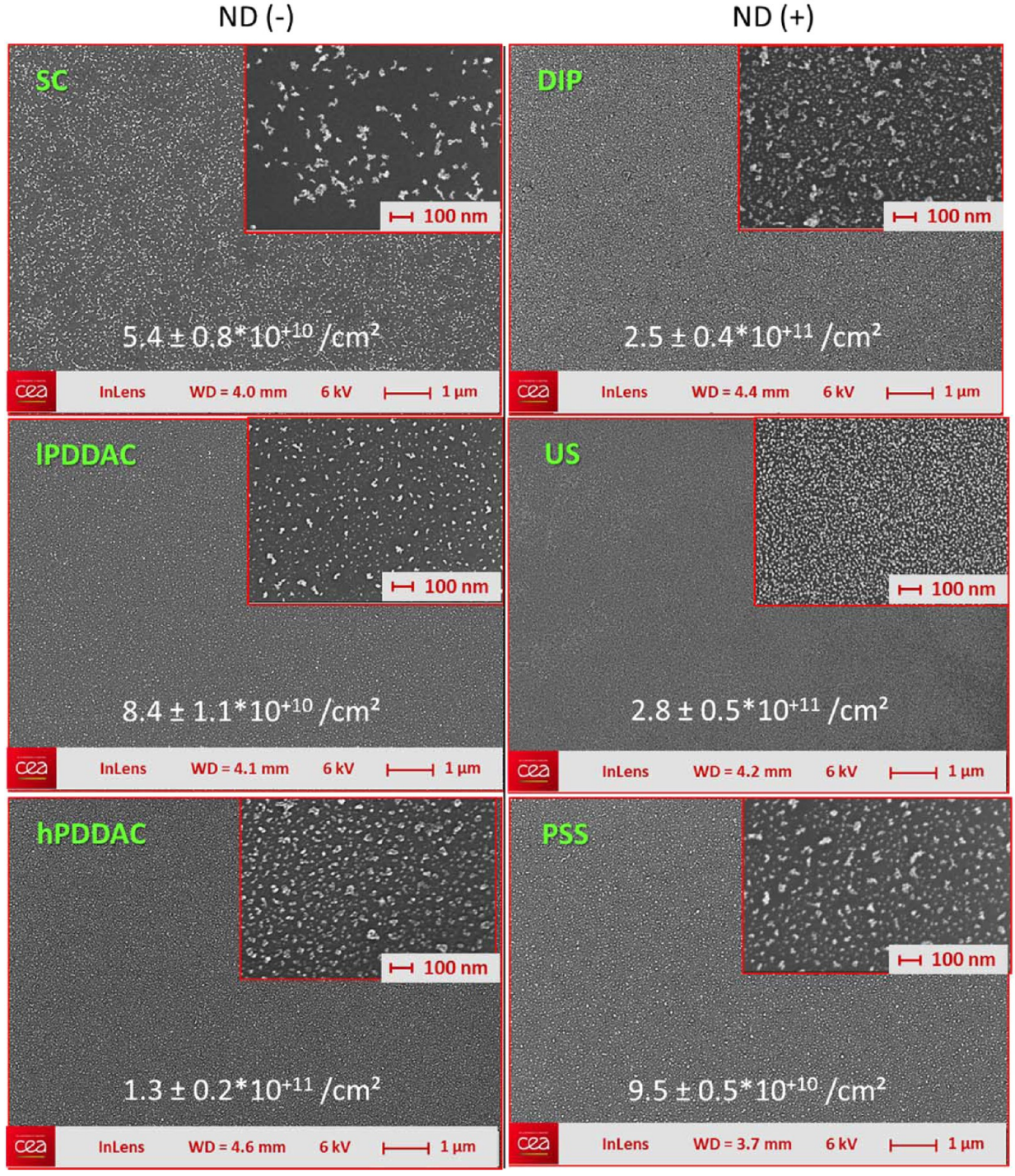

Figure 3. Layers prepared from (left) ND(−) and (right) ND(+). Particle densities are indicated on the images.

Nevertheless, both spectra are quite close, and thus, it is difficult to clearly establish the origin of opposite zeta potential only from the FTIR characterization. The negative zeta potential of ND is generally attributed to the presence of carboxylic acids, in the form of carboxylate ions at neutral pH, resulting from the oxidative purification and deagglomeration treatments such as heat treatment.[19] This is consistent with the HRTEM image displayed in Figure 1b, which shows that ND(−) have been submitted to intensive purification treatments. On the contrary, the surface chemistry of positively charged ND still remains an open question in the literature. On the basis of the nondiamond carbon shell visible on the HRTEM image (Figure 1a), the hypothesis on the formation of endoperoxides on small sp^2 islands on ND surface proposed by Petit et al.[70] seems especially relevant in the case of ND(+).

3.2. Density, Homogeneity, and Size Distribution. ND layers prepared using SC, DIP, US, hPDDAC, lPDDAC, and PSS deposition methods are shown in Figure 3. Differences in terms of density and size distribution for the same ND suspension are clearly visible on the SEM images.

SC results in the lowest density about of $5 \times 10^{+10}$ particles/cm^2 while DIP and hPDDAC samples exhibit higher densities above 10^{+11} particles/cm^2. The highest density is obtained for US samples. These observations are in accordance with

DOI: 10.1021/acsami.5b02364
ACS Appl. Mater. Interfaces 2015, 7, 15752−15764

Table 3. SEM Images of ND Layers after 1 h Sonication in Liquids[a]

Deposition method	Reference as-deposited	After 1-hour sonication in			
		Sat. KCl	Acetone	PS beads	HCl
SC	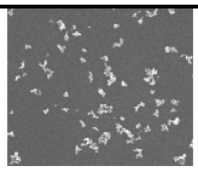	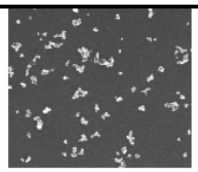	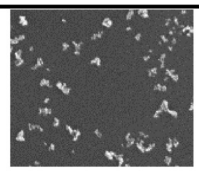	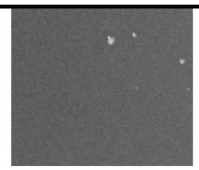	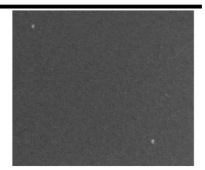
DIP	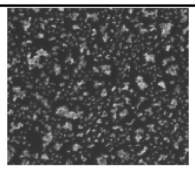	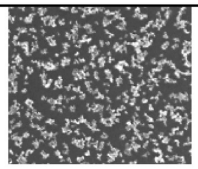	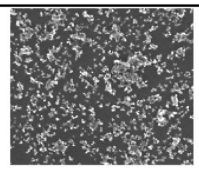	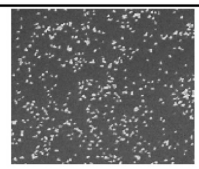	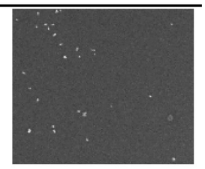
US	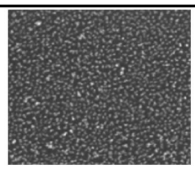	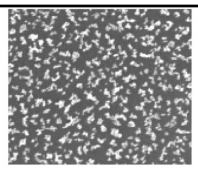	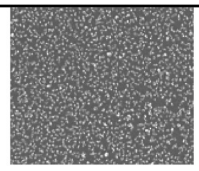	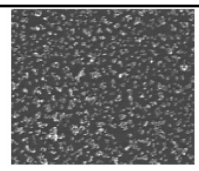	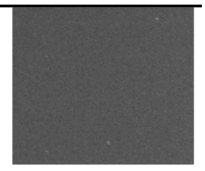
hPDDAC	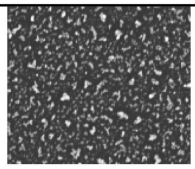	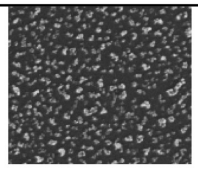	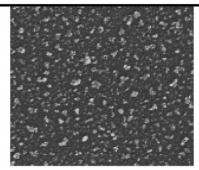	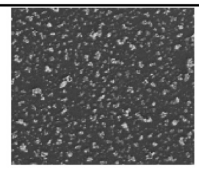	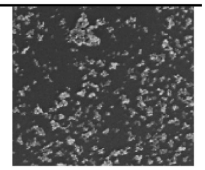
lPDDAC	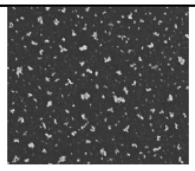	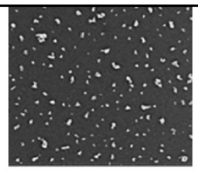	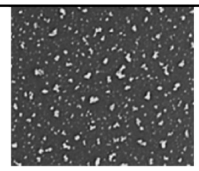	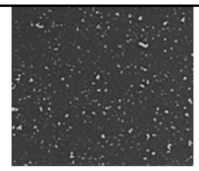	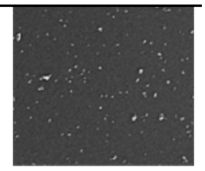
PSS	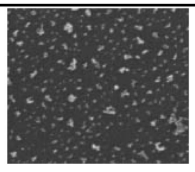	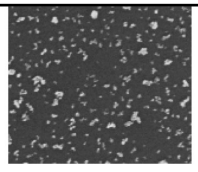	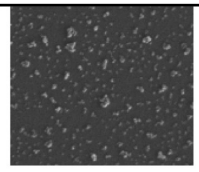	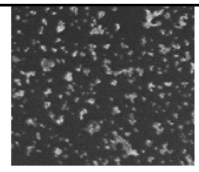	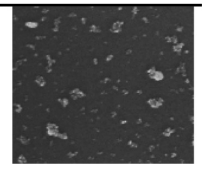

[a]Each frame is about 650 × 560 nm in size.

literature.[35−37,55] lPDDAC and PSS layers present intermediate values of density slightly lower than 10^{+11} particles/cm^2. This difference could be explained by the lower concentration of polyelectrolyte adsorbed on the surface, leading to the electrostatic self-assembly of fewer particles.

DIP, hPDDAC, lPDDAC and PSS layers are very homogeneous on the whole sample area (i.e., 1 cm^2). However, less homogeneity is obtained with SC. Both density and homogeneity for ND layers deposited by spin coating could be improved by incorporating ND into a polymer matrix (i.e., poly(vinyl alcohol)) as reported by Scorsone et al.[36] Note that although most layers prepared by US method are homogeneous, patterns at the micrometer scale may appear on some samples (Supporting Information, Figure S3).

In addition to layer density and homogeneity, the distribution of ND as isolated particles, clusters, or both when deposited on the surface must also be considered. Using SC, ND are packed into isolated small clusters. Our results for this method are very close to the ones of Tsigkourakos et al.[37] Both DIP and hPDDAC samples reveal a dense layer with mainly large clusters surrounded by very small clusters only composed of some ND. Layers prepared by US are also dense and composed of very small clusters composed of only some particles, homogeneous in size. The bubble patterns described above correspond to a local variation of density and a higher density of larger clusters similar to DIP samples. Finally, lPDDAC and PSS layers contain a higher ratio of small clusters composed of only a few particles on larger clusters compared with hPDDAC. Affoune et al. studied the electrophoretic deposition of ND layers and found that a low voltage is in favor of well-separated particles.[47] A similar phenomenon could

DOI: 10.1021/acsami.5b02364
ACS Appl. Mater. Interfaces 2015, 7, 15752−15764

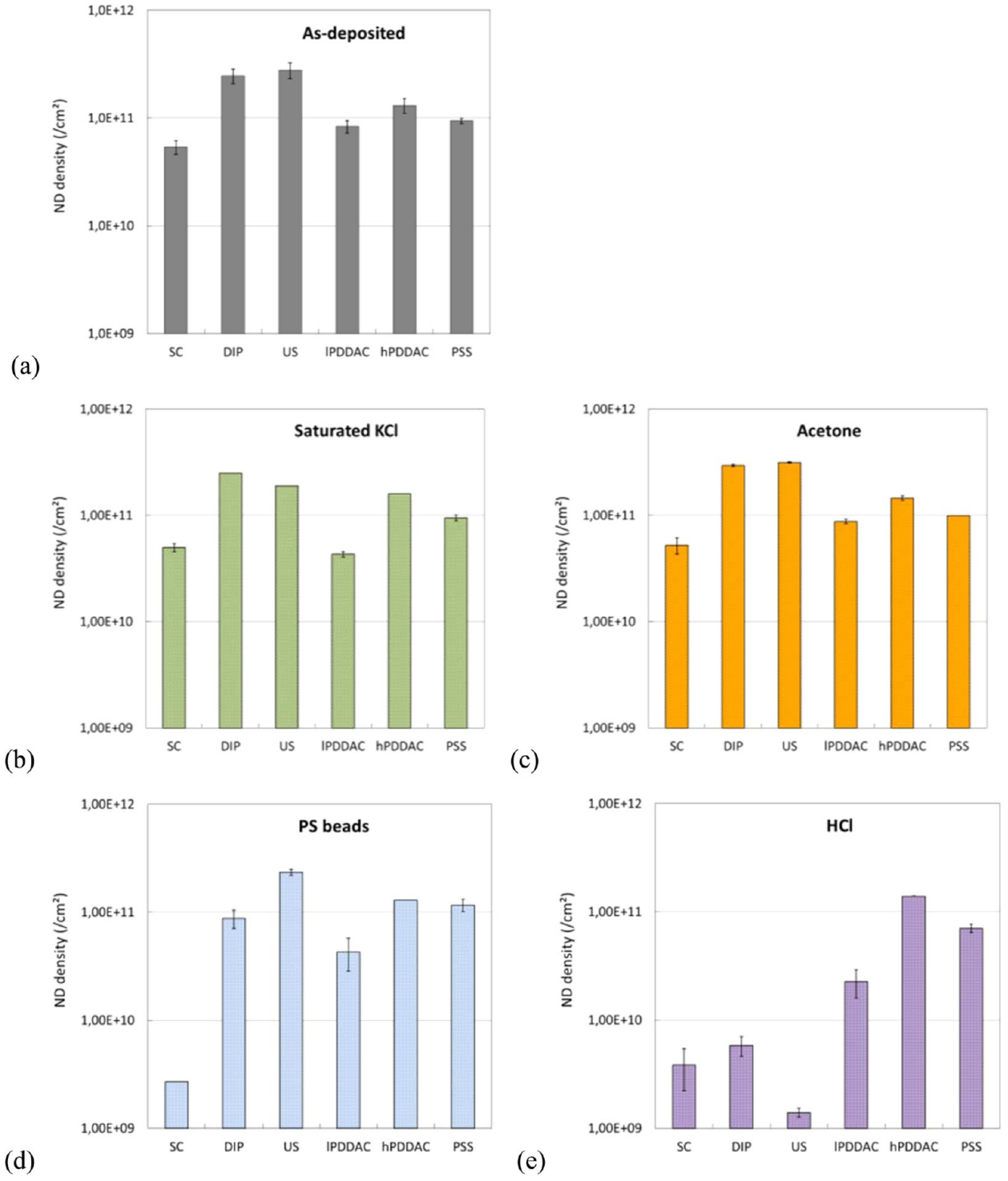

Figure 4. ND density for ND layers (a) before and after sonication in saturated (b) KCl, (c) acetone, (d) PS beads, or (e) HCl.

occur here as the surface charge is induced by the amount of adsorbed polyelectrolyte.

ND layer density, homogeneity, and size distribution strongly depend on the deposition method. This allows us to prepare four kinds of ND layers exhibiting various characteristics for the subsequent adhesion study.

3.3. Adhesion and Mobility in Liquids. In this part, we focus on ND adhesion when they are exposed to liquid media mimicking the conditions of some biological or technological applications. The test media are saturated KCl, acetone, PS beads 2 μm in diameter at 0.1 wt % in water and HCl 0.1 M to respectively assess the effects of high ionic strength, polar organic solvent, mechanical shocks against a soft material, and corrosive environment causing surface groups protonation. Samples were observed by SEM before and after sonication for 1 h in one of these media (Table 3). Images provide a qualitative evaluation of effects on layer homogeneity and particle density. Corresponding densities are given in Figure 4 for a semiquantitative evaluation.

DOI: 10.1021/acsami.5b02364
ACS Appl. Mater. Interfaces 2015, 7, 15752−15764

The results are compared here with an applicative point of view to determine which deposition method(s) is (are) the most suitable to ensure adhesion in the target environment. In saturated KCl, SC layer does not present any density and homogeneity changes. In this case, the layer is composed of ND with a negative zeta potential on a silicon sample with its native oxide having also a negative surface charge. Therefore, there is no electrostatic contribution in its adhesion. This latter is mainly ensured by van der Waals forces which are enough high to make the SC layer suitable for use in a medium with a high ionic force such as buffers or electrolytes. On the contrary, DIP and US samples were modified by sonication in the saline solution. Although particle density of the ND layer prepared by simple immersion remains unchanged, SEM observation shows a different size distribution. The smallest clusters gathered to form larger ones, more homogeneous in size. This case well illustrates the interest of combining observation with density calculation to assess not only the particle adhesion but also their mobility on the surface. Chloride and potassium ions may act as a shield around ND and even at the interface with the surface, temporarily breaking the electrostatic adhesion and allowing the particle mobility on the surface. In US layers, the very small clusters assembled in larger clusters, homogeneous in size and similar to the ones observed for DIP. A decrease of density by a third is also observed. The behavior of hPDDAC sample is similar to SC with no changes in density and mobility of small clusters to form larger ones. It is worthy to note that polyelectrolyte adsorption is considered as irreversible.[71] A quick test was performed in parallel and consisted of rinsing the sample with saturated KCl immediately after immersion into the ND colloid. hPDDAC and PSS layers are very resistant, in terms of density and homogeneity, to sonication in saturated KCl, probably because ND are partially embedded into the polyelectrolyte layer. Although ions may penetrate inside this layer and cause swelling,[72] it constitutes a protective shell at the interface. Adhesion in lPPDAC layer seems to be size dependent. Indeed, the smallest ND clusters left while the large ones remain present on the sample surface. This is coherent with the previously observed mobility of small clusters.

The test carried out in acetone investigates the effects of a polar organic solvent. DIP samples reveal a mobility of the smallest clusters aggregating with the neighboring larger ones. However, no changes in density and size distribution appear for SC, US, hPDDAC, lPDDAC, and PSS samples, similarly to sonication in saturated KCl. Because PDDAC and PSS are not soluble in acetone, the polyelectrolyte layer forms a strong protection for ND that are at least partially embedded in it. Contrary to potassium and chloride ions as previously discussed, acetone is not able to penetrate into the polyelectrolyte layer due to their insolubility in this solvent. This could explain the different behavior of ND layers deposited by electrostatic self-assembly with an intermediate polyelectrolyte layer. Except for DIP, all the deposition methods are suitable for use in acetone, that is, for lift-off processes or cleaning.

PS beads were chosen as a soft material to study the effects of mechanical shocks because this polymer has a Young's modulus of 3 MPa, close to the one of cell membranes. The diameter of the beads is 2 μm, on the same order as cells. Almost all ND deposited by SC left during this treatment. Note that the density calculated from the SEM image is not significant here, originating from some residual particles. DIP layer has lost its homogeneity, and the density is divided by a factor of 3 due to the removal of the large clusters. Only isolated small clusters are still present on the surface. The impact on US layer is reduced compared with DIP: the density remains above $2 \times 10^{+11}$ particles/cm^2, and homogeneity is conserved with a slight increase in cluster size. Both samples were prepared from the same solution (same ND source and concentration) with the same duration; the only difference lies in sonication during the deposition. Therefore, we assume that a physical anchoring would have been provided by the transfer of particle kinetic energy during the deposition under sonication, additionally to the electrostatic interactions. The resulting higher adhesion allows to the layer to resist to mechanical shocks against beads. lPDDAC density is reduced by half, due to both small and large clusters leaving off. The behavior of lPDDAC samples is closer from DIP samples because the amount of adsorbed polymer is very low. PSS and hPDDAC samples are very slightly affected by the test, with no changes in density and, respectively, a small increase in cluster size and the departure of few large clusters. They appear as the most appropriate for applications involving contact with a soft biological material such as cell manipulation.

ND adhesion becomes the most critical under exposure to acid (i.e., at pH 1). Almost all ND were removed from SC, DIP, and US samples. In the case of ND(−) deposited by SC, protonation of surface groups mainly carboxylic acids instead of carboxylate ions, change the ND zeta potential and thus electrostatic interactions with the sample surface could be strongly altered. Due to uncertain surface chemistry of ND(+), we can only assume that protons interact with some groups and have an impact on adhesion by electrostatic forces. Chloride ions may also participate to particle removal and induced mobility by shielding the positively charged ND from the negatively charged substrate and adsorption on this latter. The presence of a polyelectrolyte layer, regardless of the sign of its charge, seems to make the layer more resistant to acidic condition, maybe thanks to a partial embedding to the polymer, but the effects are still critical. lPDDAC layer density is reduced by factor 4 by the removal of the largest clusters. PSS sample shows a smaller decrease in density and larger clusters than before sonication. The density of hPDDAC does not vary significantly, but its homogeneity is strongly affected: some "holes" appeared in the layer and large aggregates formed near them, probably resulting from assembly of the depleted particles. For applications where ND layers are used in an acid environment, such as protective coatings against corrosion, adhesion is still an issue.

The first part of the study points out that adhesion of ND is more complex than simply leaving or remaining on the surface. The particles could also move and reorganize themselves as clusters. The deposition methods exhibiting the highest resistance to the tested conditions, regarding the adhesion and the mobility of ND in the layers, are electrostatic self-assembly with an intermediate PSS or PDDAC layer.

3.4. Mobility Induced by Water Microdroplets Evaporation. Even if the application requires the use of ND layers immersed into a liquid, passing through drying steps is mandatory. Another case is the use of ND layer in gases as sensors or seeding prior to CVD growth. Variation in ambient humidity and temperature may occur during sample storage. For these reasons, we further investigated the effects of air/water interfaces on ND adhesion and mobility by inducing condensation and evaporation of water microdroplets from ambient humidity on the samples.

DOI: 10.1021/acsami.5b02364
ACS Appl. Mater. Interfaces 2015, 7, 15752−15764

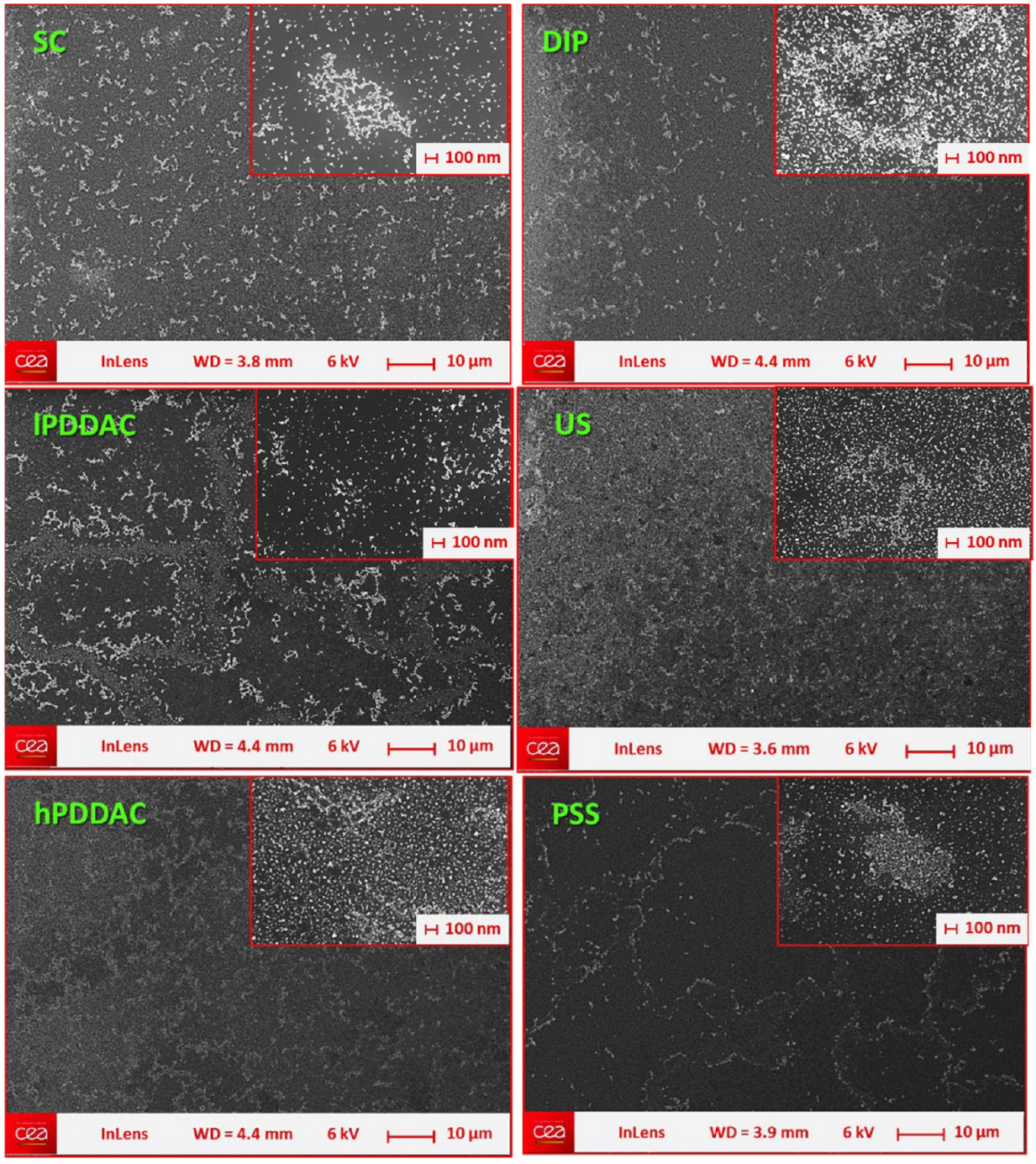

Figure 5. SEM views of ND layers exposed to condensation/evaporation of water microdroplets.

A surprising phenomenon has been evidenced for all ND layers regardless to the deposition method and the ND suspension used to prepare them. SEM observation after the microdroplet test shows the formation of aggregates and "holes", namely empty areas due to particle depletion, separated by some areas where the layer remains unmodified (Figure 5). A lower magnification reveals a pattern on the whole sample surface, about 1 cm^2, like leopard spots tens of micrometers in size. We assume that this ND mobility is driven by air/water interfaces at the micro scale. Although Lu et al. found only a slight difference in ND adhesion between the dry and wet atmospheres, they assumed that it comes from the hydrophobicity of the fluorinated particles, avoiding the water to form a meniscus.[63]

To confirm our hypothesis, water microdroplets were sprayed on hPDDAC sample and immediately dried under a high nitrogen flow so the droplets would not run over the surface. SEM observation reveals the mark of the droplets with holes inside and the presence of aggregates mainly at the edges (Figure 6). The surrounding ND layer is still homogeneous and unmodified. Here we have the case of a droplet evaporating on a nonheated hydrophilic substrate, and thus, the evaporation-induced radial flow is predominant on the Marangoni recirculation, and the particles move from the center to the edges of the droplet (Scheme 3).[73,74] This phenomenon occurs

DOI: 10.1021/acsami.5b02364
ACS Appl. Mater. Interfaces 2015, 7, 15752−15764

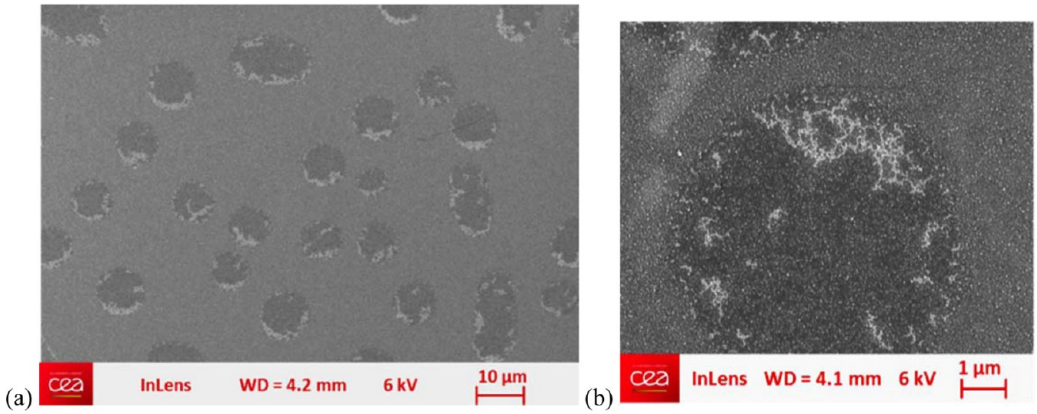

Figure 6. (a) hPDDAC sample after drying off sprayed water microdroplets and (b) a higher magnification image of the sample.

Scheme 3. Flows Competing in the Droplet for Particle Redeposition on the Surface

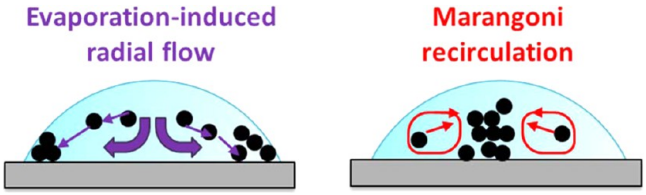

only at the micro scale. Indeed, if the layer is fully rinsed with water then dried under nitrogen flow, homogeneity is not altered. The highlighted phenomenon can also explain the pattern observed for some US samples, probably due to bubble formation during sonication (Supporting Information, Figure S3). Because the phenomenon occurs for both ND types and all deposition methods, the evaporation-induced radial flow is also predominant on van der Waals forces, H-bonding and electrostatic interactions.

4. CONCLUSION

The present study aims to provide a better knowledge of the adhesion behavior of nanoparticles layers in the real conditions they will undergo in subsequent applications. For this purpose, we developed a set of quick adhesion tests mimicking some applicative environments: sonication in saturated KCl (biological buffers), polystyrene microbeads (cells), diluted HCl (corrosion) and acetone (microfabrication processes), and condensation and evaporation of water microdroplets (sample aging, drying steps). We investigated NP layers deposited using different methods including spin-coating, electrostatic self-assembly, and layer-by-layer assembly. These techniques allowed us to prepare homogeneous layers exhibiting various characteristics in terms of density, homogeneity, and size distribution between small and large clusters. The results were analyzed using a systematic approach that quantitatively evaluates adhesion through particle density and qualitatively assesses mobility through layer homogeneity. We selected nanoparticles that are spherical, inert, and surfactant-free while available with both positive and negative zeta potential for the same diameter, as a model. Nanodiamonds meet these criteria as shown by HRTEM and FTIR characterization and are used in many applications in a growing number of fields thanks to their exceptional properties.

Because the deposition method is often based on the interactions between the NP and the substrate surface, it is also related to adhesion, and thus, it has to be carefully chosen according to the targeted application. Table 4 summarizes the results of our study. We believe that it constitutes a reference comparative study between ND deposition methods that will help to select a suitable one ensuring the good layer adhesion. From an experimental point of view, ND layers prepared using layer-by-layer methods exhibited the highest resistance in tested conditions, mainly when the adsorbed polyelectrolyte amount and thus the particle density are high. We assume that the particles are partially embedded in the polymer, protecting them. However, for some applications such as protection against corrosion, none of the used deposition methods offers enough resilience. Further adhesion improvement is required. We are currently investigating different kinds of post-treatments for this purpose. They will be detailed in a forthcoming article.

Table 4. Suitable Deposition Methods for Each Tested Condition and Related Applications

test condition	example of application	suitable deposition methods
saturated KCl	use in biological buffers	SC, hPDDAC, PSS
acetone	lift-off, cleaning	SC, US, hPDDAC, lPDDAC, PSS
PS beads	cell culture	US, hPDDAC, PSS
HCl 0.1 M	protection against corrosion	none
water microdroplets	sample aging, drying	none

The results obtained here complete the current literature on ND adhesion but are not limited to this material. Furthermore, it reveals that NP adhesion is, in fact, more complex than simply leaving or remaining on the surface. The particles could also move and reorganize themselves as clusters. We highlighted, in particular, a surprising mobility during condensation and evaporation of water microdroplets, driven by air/water interfaces. Comparison with other reference nanomaterials would confirm if the highlighted phenomena could be extended to any kind of nanoparticles layers.

■ ASSOCIATED CONTENT

Supporting Information

Particle size distribution and zeta potential of ND colloids measured by DLS, FTIR spectra before pellet drying, and SEM images of the prepared ND layers at a low magnification. The

DOI: 10.1021/acsami.5b02364
ACS Appl. Mater. Interfaces 2015, 7, 15752−15764

Supporting Information is available free of charge on the ACS Publications website at DOI: 10.1021/acsami.5b02364.

AUTHOR INFORMATION

Corresponding Author

* Tel.: +33(0)169 084 760. Fax: +33(0)169 088 965. E-mail: hugues.girard@cea.fr.

Author Contributions

The manuscript was written through contribution of all authors. All authors have given approval to the final version of the manuscript.

Funding

This work was supported by the French Funding Agency (ANR), by means of the Opt-Spect-HS-AFM project (ANR-12-BS10-0009).

Notes

The authors declare no competing financial interest.

ACKNOWLEDGMENTS

A special thank is addressed to Eiji Ōsawa from NanoCarbon Research Institute in Japan for providing the ND(+) colloid. The authors are grateful to Bogdan Palosz from the Institute of High Pressure Physics in Warsaw, Poland, and to Olga Shenderova from Adámas Nanotechnologies and International Center of Technology, Raleigh, NC, for permission to reprint HRTEM image of ND(−). We thank Mohammed Sennour from Centre des Matériaux MINES Paristech for HRTEM observation of ND(+) and the American Physical Society for permission to reprint the corresponding image.

REFERENCES

(1) Neouze, M. A. Nanoparticle Assemblies: Main Synthesis Pathways and Brief Overview on Some Important Applications. *J. Mater. Sci.* **2013**, *48*, 7321−7349.

(2) Cao, J.; Galbraith, E. K.; Sun, T.; Grattan, K. T. V. Comparison of Surface Plasmon Resonance and Localized Surface Plasmon Resonance-Based Optical Fibre Sensors. *J. Phys.: Conf. Ser.* **2011**, *307*, 012050.

(3) Cuenya, B. R. Synthesis and Catalytic Properties of Metal Nanoparticles: Size, Shape, Support, Composition, and Oxidation State Effects. *Thin Solid Films* **2010**, *518*, 3127−3150.

(4) Carrillo, J.-M. Y.; Raphael, E.; Dobrynin, A. V. Adhesion of Nanoparticles. *Langmuir* **2010**, *26*, 12973−12979.

(5) Sun, W. Interaction Forces between a Spherical Nanoparticle and a Flat Surface. *Phys. Chem. Chem. Phys.* **2014**, *16*, 5846−5854.

(6) Kumar, A.; Staedler, T.; Jiang, X. Role of Relative Size of Asperities and Adhering Particles on the Adhesion Force. *J. Colloid Interface Sci.* **2013**, *409*, 211−218.

(7) Ranade, M. B. Adhesion and Removal of Fine Particles on Surfaces. *Aerosol Sci. Technol.* **1987**, *7*, 161−176.

(8) Xing, M.; Zhong, W.; Xu, X.; Thomson, D. Adhesion Force Studies of Nanofibers and Nanoparticles. *Langmuir* **2010**, *26*, 11809−11814.

(9) Ding, W. Micro/Nano-Particle Manipulation and Adhesion Studies. *J. Adhes. Sci. Technol.* **2008**, *22*, 457−480.

(10) Ong, Q. K.; Sokolov, I. Attachment of Nanoparticles to the AFM Tips for Direct Measurements of Interaction between a Single Nanoparticle and Surfaces. *J. Colloid Interface Sci.* **2007**, *310*, 385−390.

(11) Joo, S.; Baldwin, D. F. Interfacial Adhesion of Nano-Particle Silver Interconnects for Electronics Packaging Application. In *Proc. - Electron. Compon. Technol. Conf.*, Lake Buena Vista, FL, May 27−30, **2008**; 1417−1423.10.1109/ECTC.2008.4550163

(12) Guelorget, B.; Toury, T.; Shen, H.; Lamy de la Chapelle, M. A New Semi-Quantitative Scratch-Test Method to Assess the Adhesion of Gold Nanoparticles on Glass for Ultrasensitive Chemical and Biochemical Sensors. *Scr. Mater.* **2012**, *67*, 515−518.

(13) P. Leiderer, M.; Olapinski, M.; Mosbacher, J. B. Nanoparticle Adhesion and Removal Studied by Pulsed Laser Irradiation. *Proc. SPIE* **2006**, *6261*, 62610F.

(14) Lin, J.; Cetinkaya, C. Potential Thermo-Mechanical Substrate Damage in Nanoparticle Removal with Pulsed Lasers. *J. Adhes. Sci. Technol.* **2003**, *17*, 91−113.

(15) Fang, X.; Mao, J.; Levin, E. M.; Schmidt-rohr, K. Nonaromatic Core - Shell Structure of Nanodiamond from Solid-State NMR Spectroscopy. *J. Am. Chem. Soc.* **2009**, *131*, 1426−1435.

(16) Krueger, A. The Structure and Reactivity of Nanoscale Diamond. *J. Mater. Chem.* **2008**, *18*, 1485−1492.

(17) Ozawa, M.; Inaguma, M.; Takahashi, M.; Kataoka, F.; Krüger, A.; Ōsawa, E. Preparation and Behavior of Brownish, Clear Nanodiamond Colloids. *Adv. Mater.* **2007**, *19*, 1201−1206.

(18) Mochalin, V. N.; Shenderova, O.; Ho, D.; Gogotsi, Y. The Properties and Applications of Nanodiamonds. *Nat. Nanotechnol.* **2012**, *7*, 11−23.

(19) Krueger, A.; Lang, D. Functionality Is Key: Recent Progress in the Surface Modification of Nanodiamond. *Adv. Funct. Mater.* **2012**, *22*, 890−906.

(20) Yu, S.-J.; Kang, M.-W.; Chang, H.-C.; Chen, K.-M.; Yu, Y.-C. Bright Fluorescent Nanodiamonds: No Photobleaching and Low Cytotoxicity. *J. Am. Chem. Soc.* **2005**, *127*, 17604−17605.

(21) Fu, C.-C.; Lee, H.-Y.; Chen, K.; Lim, T.-S.; Wu, H.-Y.; Lin, P.-K.; Wei, P.-K.; Tsao, P.-H.; Chang, H.-C.; Fann, W. Characterization and Application of Single Fluorescent Nanodiamonds as Cellular Biomarkers. *Proc. Natl. Acad. Sci. U. S. A.* **2007**, *104*, 727−732.

(22) Vaijayanthimala, V.; Chang, H.-C. Functionalized Fluorescent Nanodiamonds for Biomedical Applications. *Nanomedicine (London, U. K.)* **2008**, *4*, 47−55.

(23) Freitas, R. A. Is Diamond Biocompatible with Cells. *Institute for Molecular Manufacturing Reports* [Online] 1999, *12*. http://www.imm.org/publications/reports/rep012/ (accessed June 23, 2015).

(24) Schrand, A. M.; Huang, H.; Carlson, C.; Schlager, J. J.; Omacr Sawa, E.; Hussain, S. M.; Dai, L. Are Diamond Nanoparticles Cytotoxic? *J. Phys. Chem. B* **2007**, *111*, 2−7.

(25) Amaral, M.; Dias, a G.; Gomes, P. S.; Lopes, M. a; Silva, R. F.; Santos, J. D.; Fernandes, M. H. Nanocrystalline Diamond: In Vitro Biocompatibility Assessment by MG63 and Human Bone Marrow Cells Cultures. *J. Biomed. Mater. Res., Part A* **2008**, *87*, 91−99.

(26) Burleson, T.; Yusuf, N.; Stanishevsky, A. Surface Modification of Nanodiamonds for Biomedical Application and Analysis by Infrared Spectroscopy. *Journal of Achievements in Materials and Manufacturing Engineering* **2009**, *37*, 258−263.

(27) Paget, V.; Sergent, J. A.; Grall, R.; Altmeyer-Morel, S.; Girard, H. A.; Petit, T.; Gesset, C.; Mermoux, M.; Bergonzo, P.; Arnault, J. C.; Chevillard, S. Carboxylated Nanodiamonds Are Neither Cytotoxic nor Genotoxic on Liver, Kidney, Intestine and Lung Human Cell Lines. *Nanotoxicology* **2014**, *8*, 46−56.

(28) Thalhammer, A.; Edgington, R. J.; Cingolani, L. A.; Schoepfer, R.; Jackman, R. B. The Use of Nanodiamond Monolayer Coatings to Promote the Formation of Functional Neuronal Networks. *Biomaterials* **2010**, *31*, 2097−2104.

(29) Edgington, R. J.; Thalhammer, A.; Welch, J. O.; Bongrain, A.; Bergonzo, P.; Scorsone, E.; Jackman, R. B.; Schoepfer, R. Patterned Neuronal Networks Using Nanodiamonds and the Effect of Varying Nanodiamond Properties on Neuronal Adhesion and Outgrowth. *Journal of Neural Engineering* **2013**, *10*, 056022.

(30) Ivanov, M. G.; Pavlyshko, S. V.; Ivanov, D. M.; Petrov, I.; McGuire, G.; Shenderova, O. Synergistic Compositions of Colloidal Nanodiamond as Lubricant-additive. *J. Vac. Sci. Technol., B: Nanotechnol. Microelectron.: Mater., Process., Meas., Phenom.* **2010**, *28*, 869−877.

(31) Qiao, Y.; Sun, X.; Xu, B.; Ma, S. High Temperature Tribological Behaviors of Nano-Diamond as Oil Additive. *J. Cent. South Univ. Technol. (Engl. Ed.)* **2005**, *12*, 181−185.

(32) Marko, M.; Kyle, J.; Branson, B.; Terrell, E. Tribological Improvements of Dispersed Nanodiamond in Lubricating Mineral Oil. *J. Tribol.* **2015**, *137*, 011802.
(33) Arnault, J. C.; Girard, H. A. Diamond Nucleation and Seeding Techniques: Two Complementary Strategies for Growth of Ultra-Thin Diamond Films. In *Nanodiamond*; Williams, O. A., Ed.; RSC Nanoscience & Nanotechnology; Royal Society of Chemistry: London, 2014; pp 221−252.
(34) Daenen, M.; Williams, O. A.; D'Haen, J.; Haenen, K.; Nesládek, M.; Seeding. Growth and Characterization of Nanocrystalline Diamond Films on Various Substrates. *Phys. Status Solidi A* **2006**, *203*, 3005−3010.
(35) Williams, O. A.; Douhéret, O.; Daenen, M.; Haenen, K.; Ōsawa, E.; Takahashi, M. Enhanced Diamond Nucleation on Monodispersed Nanocrystalline Diamond. *Chem. Phys. Lett.* **2007**, *445*, 255−258.
(36) Scorsone, E.; Saada, S.; Arnault, J. C.; Bergonzo, P. Enhanced Control of Diamond Nanoparticle Seeding Using a Polymer Matrix. *J. Appl. Phys.* **2009**, *106*, 014908.
(37) Tsigkourakos, M.; Hantschel, T.; Janssens, S. D.; Haenen, K.; Vandervorst, W. Spin-Seeding Approach for Diamond Growth on Large Area Silicon-Wafer Substrates. *Phys. Status Solidi A* **2012**, *209*, 1659−1663.
(38) Girard, H. A.; Perruchas, S.; Gesset, C.; Chaigneau, M.; Vieille, L.; Arnault, J.-C.; Bergonzo, P.; Boilot, J.-P.; Gacoin, T. Electrostatic Grafting of Diamond Nanoparticles: A Versatile Route to Nanocrystalline Diamond Thin Films. *ACS Appl. Mater. Interfaces* **2009**, *1*, 2738−2746.
(39) Almeida, C. N.; Ramos, B. C.; Da-Silva, N. S.; Pacheco-Soares, C.; Trava-Airoldi, V. J.; Lobo, A. O.; Marciano, F. R. Morphological Analysis and Cell Viability on Diamond-like Carbon Films containing Nanocrystalline Diamond Particles. *Appl. Surf. Sci.* **2013**, *275*, 258−263.
(40) Hannstein, I.; Adler, A.-K.; Lapin, V.; Osipov, V.; Opitz, J.; Schreiber, J.; Meyendorf, N. Chemically Activated Nanodiamonds for Aluminum Alloy Corrosion Protection and Monitoring. *Proc. SPIE* **2009**, *7293*, 72930O.
(41) Zhang, Q.; Mochalin, V. N.; Neitzel, I.; Hazeli, K.; Niu, J.; Kontsos, A.; Zhou, J. G.; Lelkes, P. I.; Gogotsi, Y. Mechanical Properties and Biomineralization of Multifunctional Nanodiamond-PLLA Composites for Bone Tissue Engineering. *Biomaterials* **2012**, *33*, 5067−5075.
(42) Xing, Z.; Pedersen, T. O.; Wu, X.; Xue, Y.; Sun, Y.; Finne-Wistrand, A.; Kloss, F. R.; Waag, T.; Krueger, A.; Steinmueller-Nethl, D.; Mustafa, K. Biological Effects of Functionalizing Copolymer Scaffolds with Nanodiamond Particles. *Tissue Eng., Part A* **2013**, *19*, 1783−1791.
(43) Zhang, W.; Patel, K.; Schexnider, A.; Banu, S.; Radadia, A. D. Nanostructuring of Biosensing Electrodes with Nanodiamonds for Antibody Immobilization. *ACS Nano* **2014**, *8*, 1419−1428.
(44) Chevallier, E.; Scorsone, E.; Bergonzo, P. New Sensitive Coating Based on Modified Diamond Nanoparticles for Chemical SAW Sensors. *Sens. Actuators, B* **2011**, *154*, 238−244.
(45) Cuche, A.; Sonnefraud, Y.; Faklaris, O.; Garrot, D.; Boudou, J.-P.; Sauvage, T.; Roch, J.-F.; Treussart, F.; Huant, S. Diamond Nanoparticles as Photoluminescent Nanoprobes for Biology and near-Field Optics. *J. Lumin.* **2009**, *129*, 1475−1477.
(46) Astuti, Y.; Poolton, N. R. J.; Butenko, Y. V.; Šiller, L. Evaporation and Alignment of 1-Undecene Functionalised Nanodiamonds. *J. Lumin.* **2014**, *156*, 41−48.
(47) Affoune, A. M.; Prasad, B. L. V; Sato, H.; Enoki, T. Electrophoretic Deposition of Nanosized Diamond Particles. *Langmuir* **2001**, *17*, 547−551.
(48) Schmidlin, L.; Pichot, V.; Josset, S.; Pawlak, R.; Glatzel, T.; Kawai, S.; Meyer, E.; Spitzer, D. Two-Dimensional Nanodiamond Monolayers Deposited by Combined Ultracentrifugation and Electrophoresis Techniques. *Appl. Phys. Lett.* **2012**, *101*, 253111.
(49) Shenderova, O.; Hens, S.; McGuire, G. Seeding Slurries Based on Detonation Nanodiamond in DMSO. *Diamond Relat. Mater.* **2010**, *19*, 260−267.
(50) Fox, O. J. L.; Holloway, J. O. P.; Fuge, G. M.; May, P. W.; Ashfold, M. N. R. Electrospray Deposition of Diamond Nanoparticle Nucleation Layers for Subsequent CVD Diamond Growth. *MRS Online Proc. Libr.* **2009**, *1203*, J17−J27.
(51) Girard, H. A.; Scorsone, E.; Saada, S.; Gesset, C.; Arnault, J. C.; Perruchas, S.; Rousseau, L.; David, S.; Pichot, V.; Spitzer, D.; Bergonzo, P. Electrostatic Grafting of Diamond Nanoparticles towards 3D Diamond Nanostructures. *Diamond Relat. Mater.* **2012**, *23*, 83−87.
(52) Lee, S.-K.; Kim, J.-H.; Jeong, M.-G.; Song, M.-J.; Lim, D.-S. Direct Deposition of Patterned Nanocrystalline CVD Diamond Using an Electrostatic Self-Assembly Method with Nanodiamond Particles. *Nanotechnology* **2010**, *21*, 505302.
(53) Kim, J. H.; Lee, S. K.; Kwon, O. M.; Hong, S. I.; Lim, D. S. Thickness Controlled and Smooth Polycrystalline {CVD} Diamond Film Deposition on SiO2 with Electrostatic Self Assembly Seeding Process. *Diamond Relat. Mater.* **2009**, *18*, 1218−1222.
(54) Hongthani, W.; Fermín, D. J. Layer-by-Layer Assembly and Redox Properties of Undoped HPHT Diamond Particles. *Diamond Relat. Mater.* **2010**, *19*, 680−684.
(55) Hees, J.; Kriele, A.; Williams, O. A. Electrostatic Self-Assembly of Diamond Nanoparticles. *Chem. Phys. Lett.* **2011**, *509*, 12−15.
(56) Liu, Y.; Khabashesku, V. N.; Halas, N. J. Fluorinated Nanodiamond as a Wet Chemistry Precursor for Diamond Coatings Covalently Bonded to Glass Surface. *J. Am. Chem. Soc.* **2005**, *127*, 3712−3713.
(57) Guan, B.; Wu, L.; Ren, B.; Zhi, J. An Easy Method for Attaching Nanodiamond Particles to Amine Active Glass-like Carbon. *Carbon* **2006**, *44*, 2858−2860.
(58) Wang, H.-D.; Yang, Q.; Niu, C. H.; Badea, I. Protein-Modified Nanodiamond Particles for Layer-by-Layer Assembly. *Diamond Relat. Mater.* **2011**, *20*, 1193−1198.
(59) Zhuang, H.; Song, B.; Staedler, T.; Jiang, X. Microcontact Printing of Monodiamond Nanoparticles: An Effective Route to Patterned Diamond Structure Fabrication. *Langmuir* **2011**, *27*, 11981−11989.
(60) Vandenryt, T.; Grieten, L.; Janssens, S. D.; van Grinsven, B.; Haenen, K.; Ruttens, B.; D'Haen, J.; Wagner, P.; Thoelen, R.; De Ceuninck, W. Rapid Fabrication of Micron-Sized CVD-Diamond Structures by Microfluidic Contact Printing. *Phys. Status Solidi A* **2014**, *211*, 1448−1454.
(61) Fox, N. A.; Youh, M. J.; Steeds, J. W.; Wang, W. N. Patterned Diamond Particle Films. *J. Appl. Phys.* **2000**, *87*, 8187−8191.
(62) Chen, Y.-C.; Tzeng, Y.; Cheng, A.-J.; Dean, R.; Park, M.; Wilamowski, B. M. Inkjet Printing of Nanodiamond Suspensions in Ethylene Glycol for CVD Growth of Patterned Diamond Structures and Practical Applications. *Diamond Relat. Mater.* **2009**, *18*, 146−150.
(63) Lu, H.; Goldman, J.; Ding, F.; Sun, Y.; Pulikkathara, M. X.; Khabashesku, V. N.; Yakobson, B. I.; Lou, J. Friction and Adhesion Properties of Vertically Aligned Multi-Walled Carbon Nanotube Arrays and Fluoro-Nanodiamond Films. *Carbon* **2008**, *46*, 1294−1301.
(64) Aravind, V. R.; Lutkus, L.; Legum, B. Adhesion in Nanodiamond Particles. In *Bull. Am. Phys. Soc.*, Proceedings of the APS March Meeting, Baltimore, MD, March 18−22, **2013**; *58*, B5.004. http://meetings.aps.org/link/BAPS.2013.MAR.B5.4 (accessed June 23, 2015).
(65) Lutkus, L.; Aravind, V. R.; Legum, B. Nanoscale Tribological Properties of Nanodiamond. In *Bull. Am. Phys. Soc.*, Proceedings of the APS March Meeting; Denver, CO, March 3−7, **2014**; *59*, M17.6. http://meetings.aps.org/link/BAPS.2014.MAR.M17.6 (accessed June 23, 2015).
(66) Petit, T.; Arnault, J.-C.; Girard, H. A.; Sennour, M.; Bergonzo, P. Early stages of surface graphitization on nanodiamond probed by X-ray photoelectron spectroscopy. *Phys. Rev. B: Condens. Matter Mater. Phys.* **2011**, *84*, 233407.
(67) Tu, J.-S.; Perevedentseva, E.; Chung, P.-H.; Cheng, C.-L. Size-dependent Surface CO Stretching Frequency Investigations on Nanodiamond Particles. *J. Chem. Phys.* **2006**, *125*, 174713.

DOI: 10.1021/acsami.5b02364
ACS Appl. Mater. Interfaces 2015, 7, 15752−15764

(68) Shenderova, O.; Petrov, I.; Walsh, J.; Grishko, V.; Tyler, T.; Cunnigham, V. Modification of Detonation Nanodiamonds by Heat Treatment in Air. *Diamond Relat. Mater.* **2006**, *15*, 1799−1803.
(69) Shenderova, O.; Koscheev, A.; Zaripov, N.; Petrov, I.; Skryabin, Y.; Detkov, P.; Turner, S.; Van Tendeloo, G. Surface Chemistry and Properties of Ozone-Purified Detonation Nanodiamonds. *J. Phys. Chem. C* **2011**, *115*, 9827−9837.
(70) Petit, T.; Arnault, J.-C.; Girard, H. A.; Sennour, M.; Kang, T.-Y.; Cheng, C.-L.; Bergonzo, P. Oxygen-hole Doping in Nanodiamond. *Nanoscale* **2012**, *4*, 6792−6799.
(71) Szilagyi, I.; Trefalt, G.; Tiraferri, A.; Maroni, P.; Borkovec, M. Polyelectrolyte Adsorption, Interparticle Forces, and Colloidal Aggregation. *Soft Matter* **2014**, *10*, 2479−2502.
(72) Dubas, S. T.; Schlenoff, J. B. Swelling and Smoothing of Polyelectrolyte Multilayers by Salt. *Langmuir* **2001**, *17*, 7725−7727.
(73) Hendarto, E.; Gianchandani, Y. B. Size Sorting of Floating Spheres Based on Marangoni Forces in Evaporating Droplets. *J. Micromech. Microeng.* **2013**, *23*, 075016.
(74) Han, W.; Byun, M.; Lin, Z. Assembling and Positioning Latex Nanoparticles via Controlled Evaporative. *J. Mater. Chem.* **2011**, *21*, 16968−16972.

DOI: 10.1021/acsami.5b02364
ACS Appl. Mater. Interfaces 2015, 7, 15752−15764